

Numerical Simulations of Flow around NAL's Non-Powered Supersonic Experimental Airplane

Minoru Yoshimoto and Takeshi Kaiden
Mitsubishi Heavy Industries, Ltd.

Abstract

CFD analyses of flow around NAL's non-powered supersonic experimental airplane are conducted. The results are compared with those of corresponding wind tunnel tests. In this paper, agreements and discrepancies between them are discussed in aspects of correspondence between calculation and test models.

1 Introduction

National Aerospace Laboratory (NAL) in Japan has designed a non-powered supersonic experimental airplane to research next generation supersonic civil transport, and the first experimental flight will be conducted in 2002.

Many wind tunnel tests were performed to estimate characteristics and performances of the plane, and some results have been opened for this competition.

In this paper, CFD analyses of flow around the experimental airplane in the flight condition and in a wind tunnel test (WTT) condition are reported. The latter is compared with results of the tests.

2 Analysis

Calculation Conditions

The calculations are conducted in two Reynolds number conditions with same free stream Mach number as follows;

1. Wind Tunnel Test (WTT) condition
Mach number : $M = 2.0$
Reynolds number : $Re = 6.44 \times 10^6$
(based on MAC of the wing)
angles of attack :
 $\alpha = -2, -1, 0, 1, 2, 3, 4, 5, 6$ [deg]
2. Flight condition
Mach number : $M = 2.0$

Reynolds number : $Re = 2.23 \times 10^7$
(based on MAC of the wing)
angles of attack :
 $\alpha = -2, -1, 0, 1, 2, 3, 4, 5, 6$ [deg]

Method

The solver used is based on thin layer Reynolds-averaged Navier-Stokes equations, and has following schemes and turbulence model:

Convection terms; Roe's flux difference splitting with MUSCL,
Viscous terms; central difference,
Time integration; LU-ADI implicit method with local time stepping,
Turbulence model; Baldwin-Lomax type.

Fully turbulence conditions are assumed for all calculations.

Grid

Single structured grid for half space is applied to every calculation. Each grid has $170 \times 161 \times 55 = 1,505,350$ points. The difference between them is in the smallest grid step, which is dependent on Reynolds number. The smallest step is set around $0.05/Re^{1/2}$ in each grid. A schematic view of grid for the wind tunnel test's condition is shown in Fig.1.

3 Results and Discussion

Lift and Pitching Moment

The lift and pitching moment characteristics are shown in Fig.2 and 3. Results of the calculations and the tests are in good agreement with each other on the whole. But small discrepancies can be found in their slopes. Test results have smaller positive slope in lift characteristic, and smaller negative slope in pitching moment

characteristic.

It is assumed that these differences are due to test model's deformation at outer portion of its wing. The outer portion of the wing is very thin and might be bent by its lift as shown in Fig. 4. The axis of moment is not parallel to the body axis, because outer wing has maximum thickness in about half chord and the half chord line is highly swept back.

One evidence of this assumption can be seen in the pressure distribution. Pressure distribution on outer wing is shown in Fig.5. At higher angles of attack (ex. $\alpha = 6^\circ$), pressure differences on upper and lower surfaces in WTT is smaller than in CFD. It means outer wing has smaller lift and smaller angle of attack in the test than in CFD.

The other stands in different point of view. Fig.6 shows slope of lift coefficient and slope of the pitching moment coefficient for several values of Mach number. There are two sets of WTT results in different facilities with a same model. At $M = 1.4$ two results of different dynamic pressure were obtained. One is almost twice as the other. The slope of lift coefficient in higher dynamic pressure is smaller than the other, and the slope of pitching moment coefficient in higher dynamic pressure is greater than the other. Relation between CFD and WTT results in $M = 2.0$ is similar to these trends. All these results are consistent at least qualitatively.

Pressure Distribution on Wing Surface

Fig.7 shows pressure distributions on other wing sections. These figures suggests that CFD results are in excellent agreement with WTT results on lower surface at positive angle of attack. But they show poor agreement on former region of upper surface. At the negative angle of attack the trend is opposite.

Fig.8 shows pressure distributions on upper surface obtained from two different scaled models' tests in different facilities. They also differ from each other at former

region.

Both two figures might show the calculation model and two test models have different sharp leading edge shapes one another. Supersonic wing with sharp leading edge may be hard to reproduce strictly in simulations and in tests of scaled models. To eliminate the uncertainty results of CFD with higher resolution and/or WTT with bigger model are expected.

Pressure Distribution on Fuselage Surface

Fig.9 shows pressure distribution on fuselage surface. CFD results are in excellent agreement with WTT results on middle region. But they are shifted each other on forebody region.

For this difference, some other estimations of the pressure at zero angle of attack can be done. Table 1 shows comparison between results of WTT, CFD, and the estimations. In the table, "CFD(fine grid)" represents CFD results for only-forebody analysis with calculation grid of fourth mean density, and "conical flow" represents a simplification of the ogive shape to cones with same semi vertexes[1], as shown in Fig.10. The table shows WTT results tend to be smaller than others. If possible, reference pressure of the measured points or some other reasons might be confirmed.

Drag

Fig.11 shows drag polar of CFD and WTT results. CFD results are in good agreement with the others. The difference is only 4 drag counts(i.e. $\Delta C_D = 0.0004$). The value of 4 drag counts may not be only due to CFD error but WTT error. Trips around the leading edge of the model may produce additional unexpected drag (not by transition) of similar magnitude in supersonic WTT [3].

If there were no such error, they would show excellent agreement in spite of model's deformation as mentioned above. That is because the deformation gives no effect on the drag polar shape and plots in the polar

are only translated along the curve [3].

Fig.12 shows CFD results of two Reynolds number conditions. They differ about 10 drag counts for all lift coefficients. This difference is only due to friction drag difference. It can be made sure of by a simple estimation of substitution for friction on a flat plate [4], and the result is 11 drag counts. They agree well with each other.

4 Conclusion

- Results of CFD and WTT show good agreement on the whole.
- There is a possibility of aeroelastic deformation occurring at outer portion of the wing.
- WTT with measurement of wing deformation and calculation of deformed test model are expected to make sure of CFD accuracy.

References

- [1] "Equations, Tables, and Charts for Compressible Flow", NACA Rep. 1135, 1953
- [2] "Pressure Distribution on Forebodies and Afterbodies of Revolution at Zero Incidence in Inviscid Flow", ESDU Bodies S.05.03.01
- [3] Mejia, K. M., "A Comprehensive Review of High Speed Wind Tunnel Performance Data from the Boeing High Speed Civil Transport Program", AIAA-2001-0453
- [4] Hoerner, S. F., *Fluid Dynamic Drag*, 1958

Table 1 Estimations of Pressure on Forebody Surface at Zero Angle of attack

X/L	0.1	0.25
δ	5.1°	2.6°
WTT	0.007	-0.010
CFD	0.030	0.003
Cp		
CFD(fine grid)	0.030	0.003
conical flow ¹	0.035	0.010
ESDU ²	0.045	-0.014

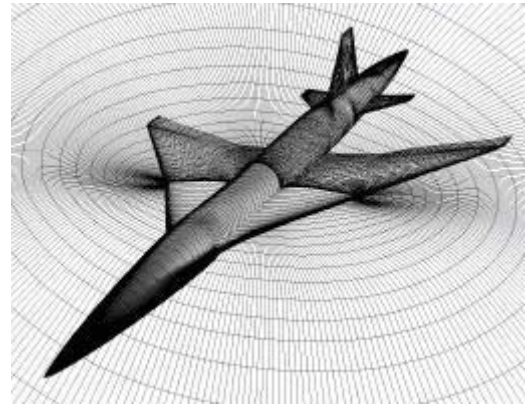


Fig.1 Single Structured Grid

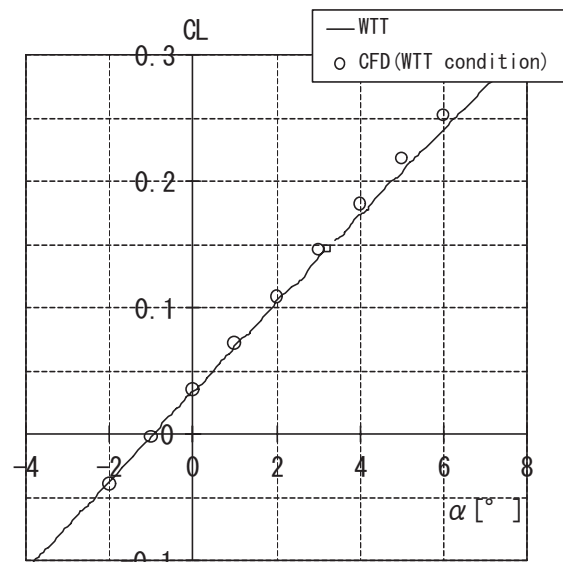


Fig.2 Lift Coefficient

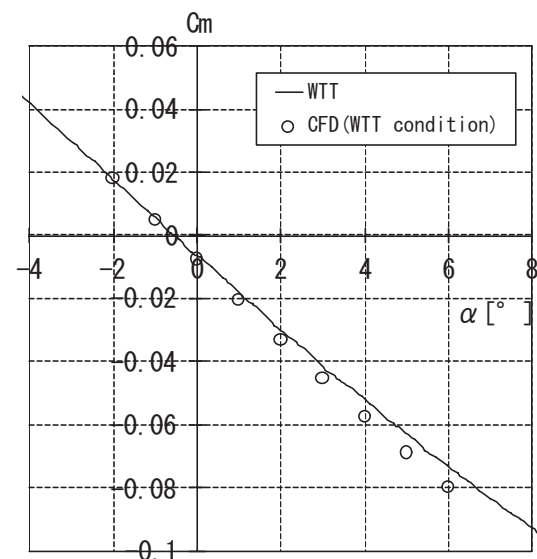


Fig.3 Pitching Moment Coefficient

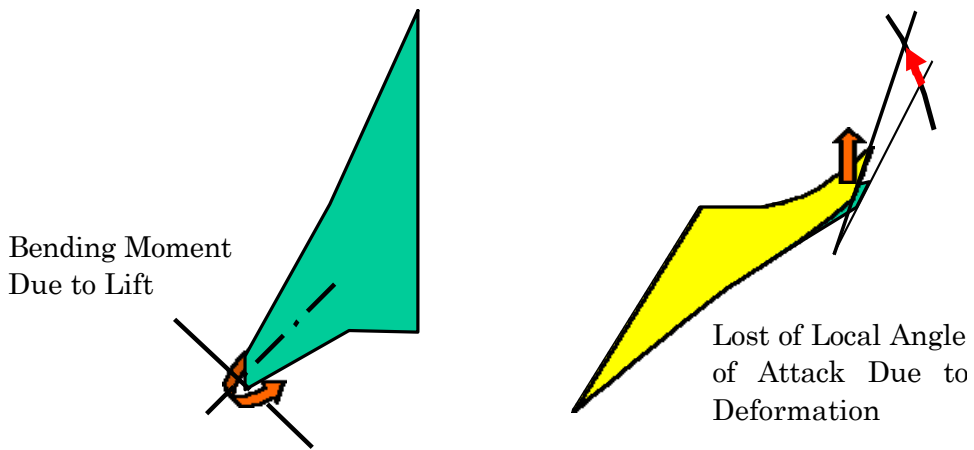


Fig.4 Aeroelastic Deformation of Outer Wing

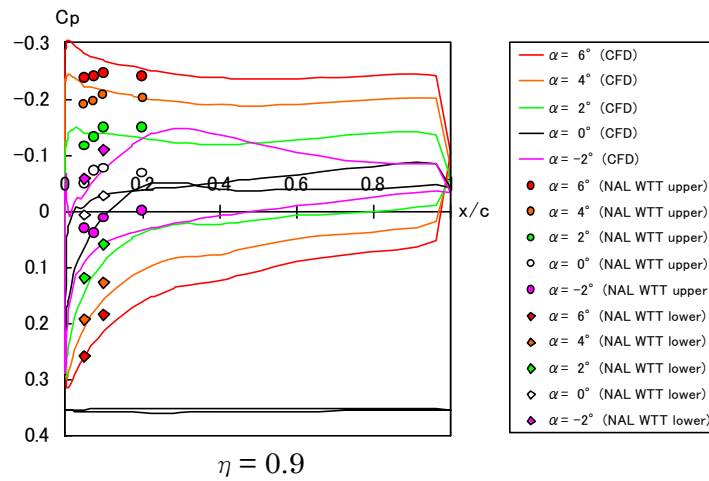


Fig.5 Pressure Distribution on Outer Wing

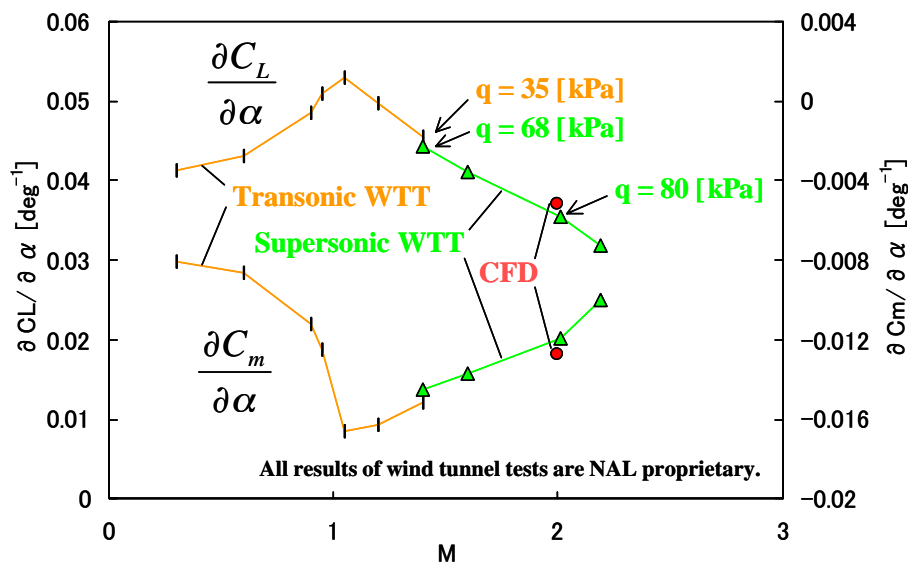


Fig.6 Discrepancies of Lift and Pitching Moment Slope between Different Dynamic Pressure

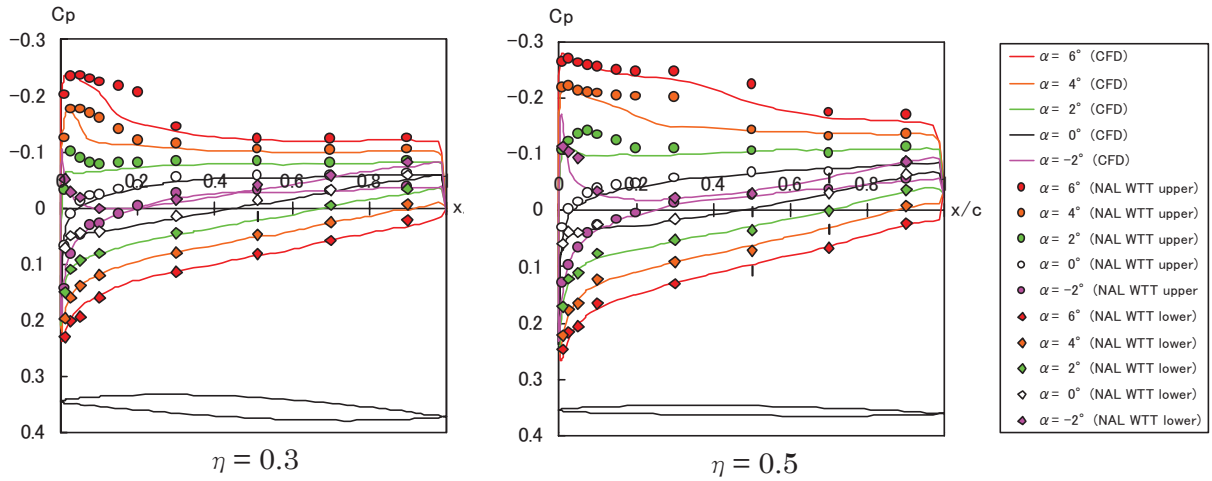


Fig.7 Pressure Distribution on Wing Surface in CFD and WTT

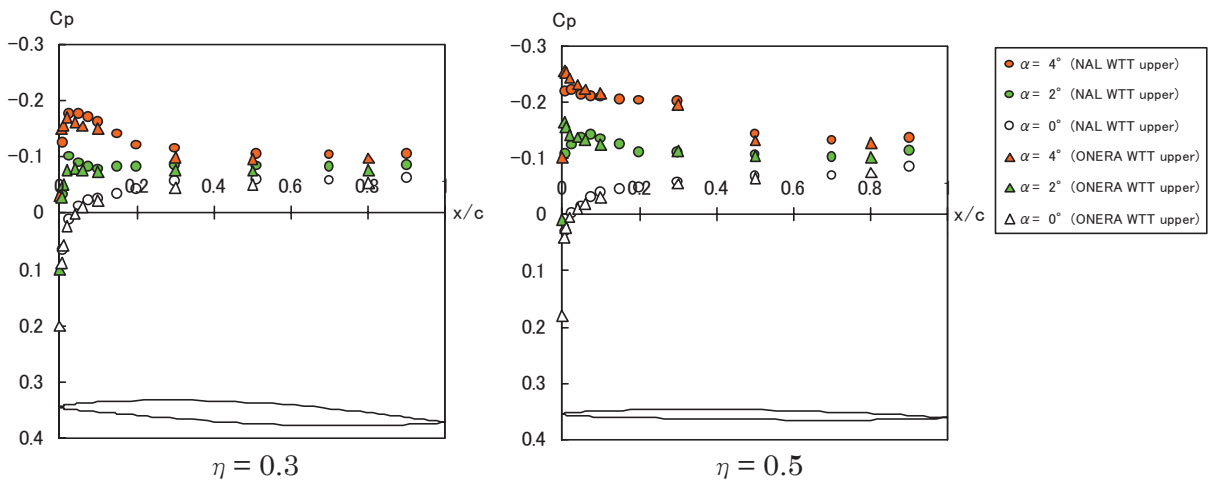


Fig.8 Pressure Distribution on Wing Surface of Different Models in Different Facilities

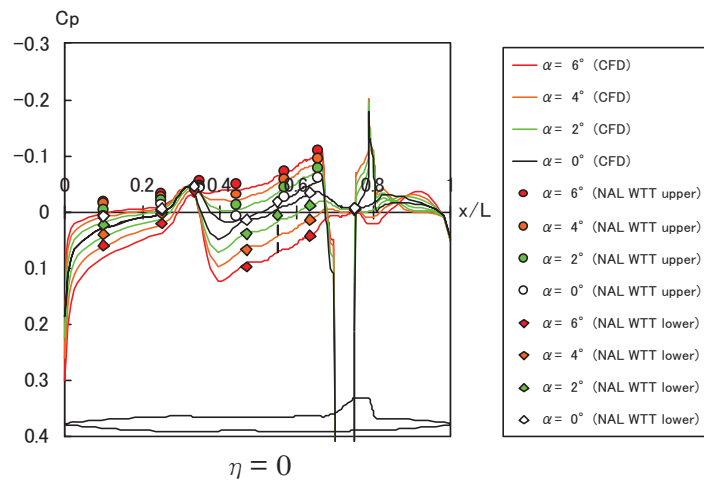


Fig.9 Pressure Distribution on Fuselage Surface in CFD and WTT

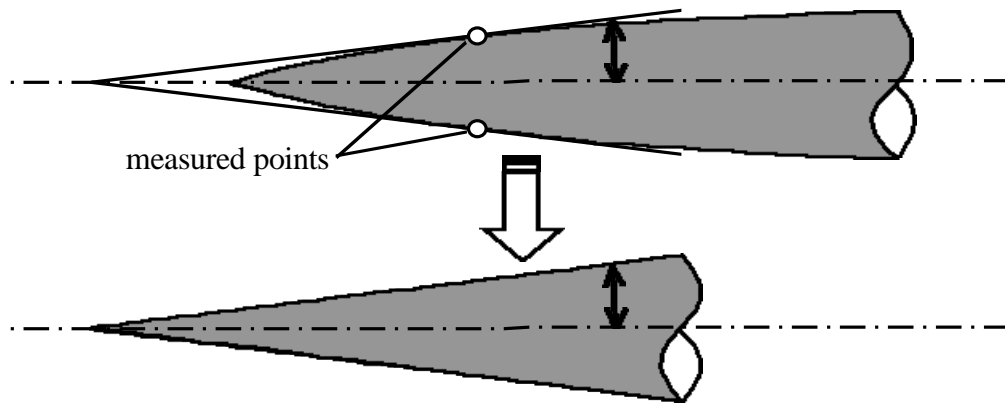


Fig.10 Simplification of Ogive Shape to Cone for Rough Estimation of Fuselage Pressure

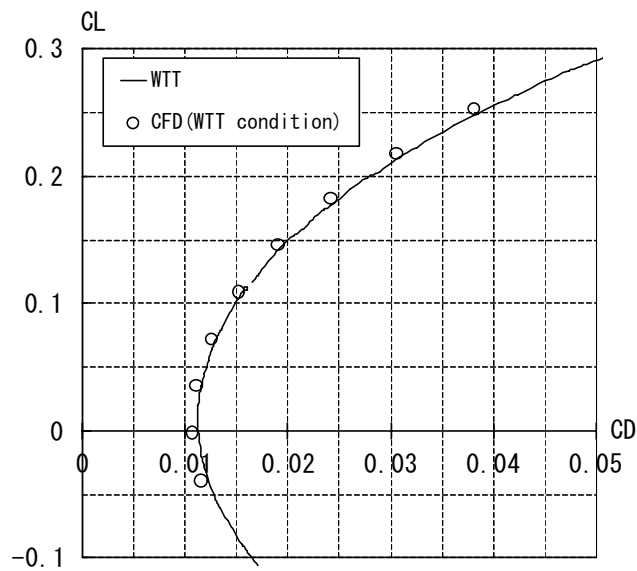


Fig.11 Drag Polar in WTT condition (No integration on the boat tail surface in CFD results.)

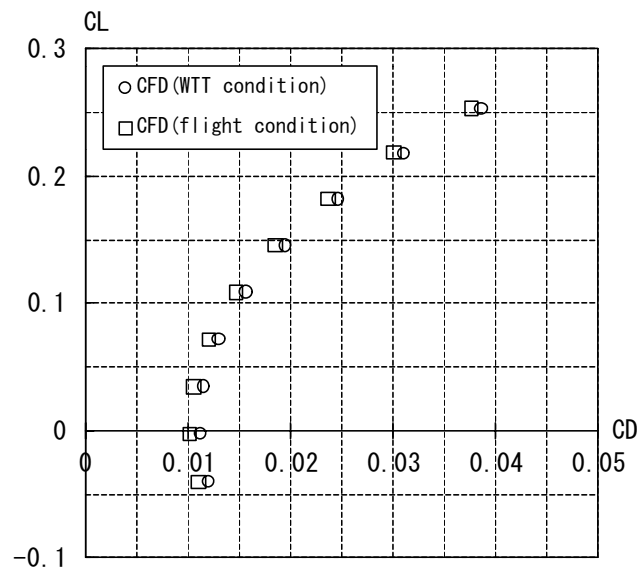


Fig.12 Drag Polar in Different Reynolds Number Conditions